EPJ Web of Conferences **340**, 10022 (2025) https://doi.org/10.1051/epjconf/202534010022
Powders & Grains 2025

Using x-ray rheography to estimate the 3D field of inertial numbers in flowing granular media

Andres Escobar[1,2,*], *James* Baker[2,3,**], *François* Guillard[2,***], *Thierry* Faug[1,****], and *Itai* Einav[2,†]

[1]Université Grenoble Alpes, CNRS, INRAE, IRD, Grenoble INP, IGE, 38000 Grenoble, France
[2]School of Civil Engineering, The University of Sydney, Sydney, NSW 2006, Australia
[3]School of Computer Science and Mathematics, Liverpool John Moores University, Liverpool, L3 3AF, UK

Abstract. The rheology of granular materials is commonly described using the inertial number (I) as a measure of their fluidity. As the ratio between the time of macroscopic deformation and the time of microscopic rearrangement, I depends on the shear strain rate within the medium, which can vary in space. With dry granular media being opaque, experimental measurements of the field of inertial numbers were mainly limited to two-dimensional (2D) observations along transparent walls in three-dimensional (3D) systems. This work addresses this gap using dynamic x-ray rheography of continuously flowing granular materials through an open channel conveyor belt setup. The granular medium is driven towards a perpendicular wall and forms a steady heap, for which the velocity field along the belt direction is measured in 3D. When used to estimate the shear strain rate, it is shown that, under the heap, a marked 3D pattern develops in the spatial distribution of I. The experimental findings are cross-validated with discrete element method simulations.

1 Introduction

The interaction of granular flows with obstacles tends to produce complex internal dynamics that are often identified through non-trivial variations in the free surface. Examples include surface undulations in large avalanche deposits and collective motion of particles [1, 2]. The rheology of these flows is commonly analysed using concepts based on the inertial number (I) [3], or the granular temperature [4] that could be measured in 3D as in [5]. In particular, I is often used to demarcate transitions (commonly reported at $I \sim 10^{-3}$ [6]) between quasi-static (QS) and inertial regimes of steady granular flows, and to detect intensive shear zones. However, experimental measurements of I are generally limited to 2D setups [7] or observations at the boundaries of 3D systems [8]. There are a few experiments in 3D using x-ray tomography but these need to halt the flow and are thus limited to the analysis of consecutive sets of relaxed states [9, 10]. Measurements of continuously flowing grains pose significant challenges in 3D setups due to the opacity of the grains and the limitations of traditional imaging techniques.

To overcome these limitations, this study employs dynamic x-rays on a steady granular heap produced in an open channel by transporting granular material with a conveyor belt towards an obstacle. The recorded radiographs are used to measure the internal velocity fields and the 3D free surface, from which I is estimated, given an assumed hydrostatic stress field. A complementary discrete element method (DEM) simulation is also performed to validate the I measurements. This setup has been previously used to study internal velocities, unveiling complex internal dynamics [11]. This paper will focus on experimentally estimating the 3D field of I within the bulk of the flow.

The paper is organised as follows. Section 2 summarises the experimental setup and procedures, as well as the corresponding DEM model. Section 3 shows the results with a focus on the fields of velocity and inertial number within the bulk, obtained both using the x-ray tests and the DEM simulations. Finally, Section 4 discusses the main findings and perspectives.

2 Methods

2.1 Experimental setup

The experimental setup consists of an open channel placed over a rubber conveyor belt. The belt drives grains that leave a reservoir through a gap with a fixed height (h_1) and velocity (U_b) towards a perpendicular wall with another fixed gap height (h_2). Upon impact, the free surface of the moving granular medium develops a heap, as schematically represented by Fig. 1. The heap is similar to previous experimental findings that focused on the dynamics of the granular flow along boundaries [12, 13]. In our setup, the gap of height h_2 through which the grains leave the conveying system (Fig. 1) is controlled in such a way that allows the heap to reach a steady state shape when the outgoing and incoming flow rates become balanced. In

*e-mail: andres-felipe.escobar-rincon@inrae.fr
**e-mail: j.l.baker@ljmu.ac.uk
***e-mail: francois.guillard@sydney.edu.au
****e-mail: thierry.faug@inrae.fr
†e-mail: Itai.Einav@sydney.edu.au

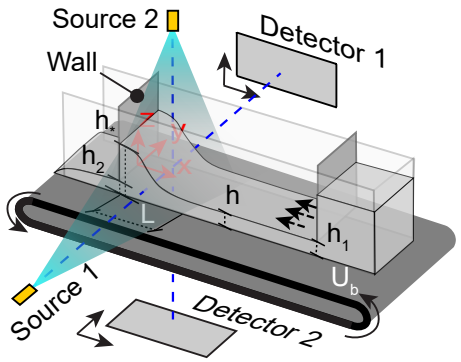

Figure 1. Overview of the conveyor belt setup with its key dimensions portrayed. Figure adapted from [11].

practice, the steady state is ensured when $h_1 \approx h_2$. As the gate heights are fixed during the test, the steady heap is produced by initially placing a pile of grains with height $> h_2$ in the flume. The free surface of the grains gradually changes before reaching the steady state heap as more grains enter the reservoir through h_1 and leave it through h_2. Eventually, as the reservoir empties and the grains leave the system, the heap vanishes.

The grains are bounded by acrylic sidewall sheets of 1 cm connected to the outgoing gate (also serving as the obstacle), which is made of aluminium. This structure is held to an external frame, leaving a small gap between the sidewall sheets above the conveyor belt to minimise undesired displacements during the test. The setup features two pairs of x-ray sources and detectors whose lines of sight are placed perpendicularly at approximately 20 cm from the setup, as displayed in Fig. 1. This orthogonal two-way x-ray apparatus captures both top and side views of the intensity variations at a frequency of 30 fps with a resolution of 960 px × 768 px at 16-bit, with a spatial resolution of 0.29 and 0.22 px mm^{-1} for detectors 1 and 2, respectively. The recorded radiographs are used to measure the free surface and internal velocities.

Here, we investigate in detail a single test of a granular flow of glass beads with a grain diameter of $d = 3 \pm 0.4$ mm. The motion is set by a belt velocity of $U_b = 2$ cm s^{-1}. The gate heights are set at $h_1 = h_2 = 2.5$ cm, and form a heap of height $h_* \approx 7.5$ cm, controlled by the height of the initial pile. In this test, the steady state was sustained for approximately 7 s. Particular details of the performed analysis are given in the upcoming subsections.

2.2 Analysis of radiographs

2.2.1 Surface detection

The steady heap can be described using a function $h(x, y)$ denoting the height of the free surface in terms of the horizontal coordinates (x, y). To reconstruct $h(x, y)$, we correlate the time-averaged absorption fields from the two detectors, assuming the radiographs follow the Beer-Lambert attenuation law [14], which describes how materials absorb radiation. The absorption fields are calculated as $\Gamma_i = < \ln(f_{r,i}/f_{0,i}) >_t$, where $f_{r,i}$ is the i -th detector's radiograph of the steady state, and $f_{0,i}$ is its corresponding radiograph of the empty chute. Here, Γ_1 provides the height of the free surface along the x-axis, and Γ_2 quantifies the intensity related to the material thickness at each x-axis position. Using these measurements, the attenuation coefficients of the flowing granular bulk are fitted, allowing us to correlate the radiograph intensity with the flow thickness. Further details of this procedure are available in [11].

2.2.2 Velocity field reconstruction

The 3D velocity field of the material within the steady heap is calculated using the x-ray rheography technique and algorithm developed in [15], which estimate the 3D velocity field by correlating the successive perpendicular radiographs of the steady flow. In this setup, only the x-axis velocity component $U_x(x, y, z)$ can be correlated as it is the only one orthogonal to the two x-ray directions. A third orthogonal x-ray may allow recovery of the other two velocity components, but only if the amount of material in its path would not be as large as in the current setup. Detector 1 captures the width-averaged velocity fields $< U_x >_y (x, z)$ and $< U_z >_y (x, z)$, and detector 2 the depth-averaged velocity fields $< U_x >_z (x, y)$ and $< U_y >_z (x, y)$. Here, the notation of $< U_x >_y (x, z)$ means the width average of the x-direction velocities along the y-coordinate for different x and z coordinates, etc. The radiographs used for rheography are normalised to highlight the velocity variations inside the bulk. This is produced by dividing each detector's (i) radiograph $(f_{r,i})$ of the steady state regime by their time average as $(\ln(f_{r,i}/ < f_{r,i} >_t))$. The velocity fields are reconstructed using an interrogation window of 32 px with a maximum displacement of 16 px per frame. The obtained velocity field is then trimmed using the reconstructed free surface.

2.3 Numerical simulations

A DEM simulation using YADE [16] is performed to validate the experimental results and complement them by inferring the remaining velocity components in the volume (U_y, U_z). The simulation uses spherical particles to model the glass beads used in the experiments. The spheres' interactions are modelled using a viscoelastic contact law with a Coulomb frictional threshold for tangential forces [17]. The particles with parameters typically used in glass beads. They have a restitution coefficient of 0.5, density of 2500 kg m^{-3}, and an interparticle friction coefficient of 0.5. The boundaries of the granular bulk (walls, obstacle and belt) have a mean friction coefficient of 1.0. Sidewalls are reproduced using a fixed plane, and the conveyor belt is made of fixed rows of spheres at the bottom to mimic the rough conveyor belt with a speed U_b. They share the same contact properties as the grains in the bulk, but with a higher friction coefficient. A snapshot of the simulation is shown in Fig. 2. The simulation progresses until steady state, and the information in this state is averaged in time and space using the coarse-graining procedure [18, 19] with a Lucy radius of $1.5d$.

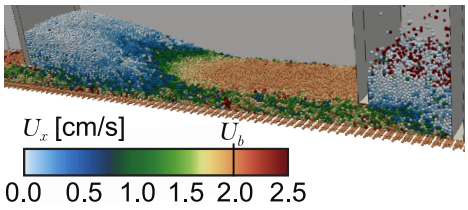

Figure 2. Snapshot of the simulation. The sidewall facing the viewer is set transparent for visualisation purposes.

2.4 Inertial number

The local inertial number is defined as

$$I(x,y,z) = \frac{\dot{\gamma}(x,y,z)d}{\sqrt{P(x,y,z)/\rho_p}}, \quad (1)$$

where $\dot{\gamma}$ is a second invariant of the strain rate tensor, defined as $\sqrt{\varepsilon_{ij}\varepsilon_{ij}}$ [20], and P is the local pressure. The simulation's inertial number (I_{DEM}) is calculated using the coarse-grained velocity field to calculate $\dot{\gamma}$, and the corresponding pressure field $P = 1/3(\sigma_{xx}(x,y,z)+\sigma_{yy}(x,y,z)+\sigma_{zz}(x,y,z))$. The experimental inertial number (I_{Exp}) is estimated by considering a volume fraction of a random close packing of $\phi = 0.62$, and assuming a hydrostatic local pressure $P = \rho_p\phi(x,y,z)g(h(x,y)-z)$. The strain tensor for I_{Exp} is calculated only considering U_x (representing the primary flow), assuming the derivatives of U_y and U_z negligible. The experimental I is then given by:

$$I_{Exp} = \frac{d\sqrt{(dU_x/dy)^2 + (dU_x/dz)^2}}{\sqrt{\phi g(h-z)}}. \quad (2)$$

3 Results

3.1 3D velocity field

The reconstructed U_x velocity field in the experiment is displayed in Fig. 3, which features flow under a heap with largely two regions separated by a shear band. The velocities above the shear band are distinctively lower relative to the velocities underneath the shear band that nearly follow the belt speed U_b. Across the width, the velocities slightly reduce from the centre relative to those near the sidewalls. As grains enter the start of the heap, they form a dip in the surface. The dip is also reproduced in the simulation, as displayed in Fig. 4. The shape of the heap in the simulation resembles the experimental one, although showing a milder slope. Despite this difference, the profile of the velocity along the belt direction, U_x, resembles the experimental one, as observed in Fig. 4 (a). With this agreement between experiment and simulation in mind, the coarse-grained field from the simulation completes the picture of the flow field with the other velocity components. U_y, presented in Fig. 4 (b), displays secondary flow throughout the flume, which is particularly strong at the beginning of the heap. This somewhat explains the presence of the dip, as discussed in [11]. The vertical velocity U_z in Fig. 4 (c) displays an upstream motion at the beginning of the heap, followed by a downstream motion as the flow approaches the outgoing gate.

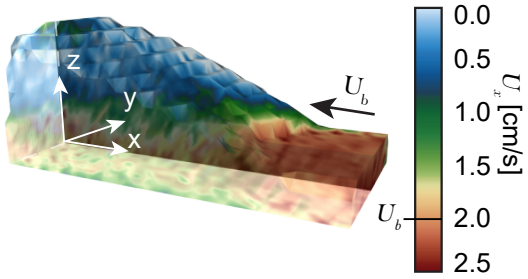

Figure 3. Velocity reconstruction of U_x using the x-ray rheography technique. Transparency is added to highlight flow along a particular xz plane.

3.2 3D inertial number field

The estimated and calculated 3D field of the inertial number in the experiment and simulation, respectively, are shown in Fig. 5. Both fields feature what might be considered as QS steady-flows near the belt, especially before the heap. The flow above the shear band in the region of the heap is also QS. Within the shear band, I goes beyond the QS regime ($I > 10^{-3}$). Similarly, I in the area of the secondary flow near the dip also appears to go beyond the QS regime. It is interesting to observe that elevated I values appear in the region of the strong secondary flow, despite their relatively low velocity compared to the primary one. The value of I near the walls is also observed to go beyond the QS regime, presumably due to the particular arrangement of particles along the walls (see Fig.1 (a) in [11]). Recall that the experimentally extracted I-field is based on an estimated stress field, which may explain part of the difference with the simulated I-field, in addition to the steeper heap slope, although one must remember that DEM is only a model. Other differences may be attributed to beam distortions as points further away from the detectors. A longer recording time is expected to mitigate these effects. A comparison of the range of inertial numbers is shown in the histograms of Fig. 6. Here, a similar distribution of I_{Exp} and I_{DEM} is observed with mean values of $< I_{Exp} >= 0.00226$ and $< I_{DEM} >= 0.00229$, beyond the QS regime. These strong similarities provide some cross-validation for both the experiment and the model.

4 Discussion and conclusions

This work introduces the first direct experimental estimation of a 3D field of inertial numbers in continuously flowing granular flows using x-ray radiography. The inertial number is estimated using only the gradients of the primary velocity component (U_x) and approximated hydrostatic stress. Despite this assumption, there is a strong agreement between the x-ray rheography experiment and the DEM simulation. Higher inertial number flows are concentrated in (1) the shear band between the top of heap and the region above the driving belt, (2) near the sidewalls, likely due to interactions with the boundary, and (3) near the dip at the start of the heap, where strong secondary flow develops. These observations highlight the benefits of

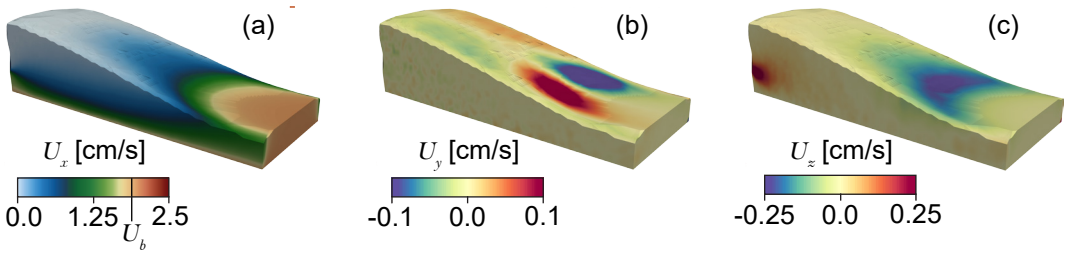

Figure 4. Coarse-grained velocity fields in the simulation. Panel (a) portrays the U_x velocity component, whereas panels (b) and (c) respectively display U_y and U_z. These velocities reveal complex secondary structures, described in [11].

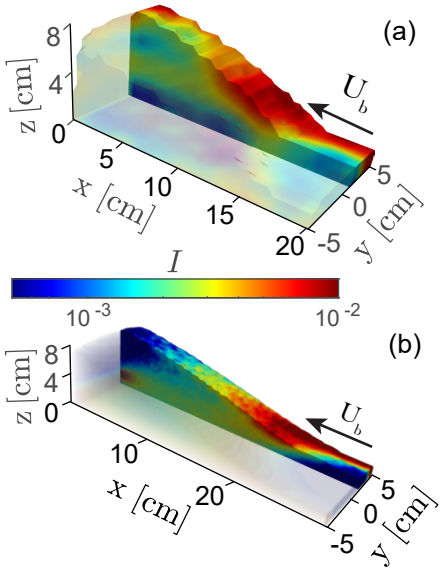

Figure 5. 3D field of inertial number: (a) x-ray experiments on the chosen *xz* plane and (b) DEM simulations on the same plane.

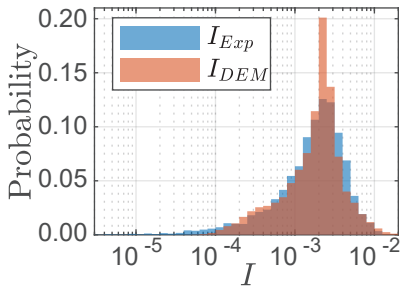

Figure 6. Probability distribution of the measured inertial number (I) for the simulation (I_{DEM}) and the experiment (I_{Exp}).

x-ray rheography for studying the internal dynamics and free surface variations of 3D granular flows.

References

[1] G. Magnarini, T.M. Mitchell, P.M. Grindrod, L. Goren, H.H. Schmitt, Nat. Commun. **10**, 4711 (2019).

[2] K. Krishnaraj, P.R. Nott, Nat. Commun. **7**, 10630 (2016).

[3] P. Jop, Y. Forterre, O. Pouliquen, Nature **441**, 727 (2006).

[4] I. Goldhirsch, Powder technology **182**, 130 (2008).

[5] Z. Maranic, F. Guillard, J. Baker, I. Einav, B. Marks, A granular thermometer, Granular Matter **23**, 1 (2021).

[6] F. da Cruz, S. Emam, M. Prochnow, J.N. Roux, F.m.c. Chevoir, Phys. Rev. E **72**, 021309 (2005).

[7] T. Miller, P. Rognon, I. Einav, in *AIP Conference Proceedings* (American Institute of Physics, 2013), Vol. 1542, pp. 483–486

[8] G. Saingier, S. Deboeuf, P.Y. Lagrée, Physics of Fluids **28** (2016).

[9] Y. Xing, J. Zheng, J. Li, Y. Cao, W. Pan, J. Zhang, Y. Wang, Physical Review Letters **126**, 048002 (2021).

[10] Y. Yuan, Z. Zeng, Y. Xing, H. Yuan, S. Zhang, W. Kob, Y. Wang, Nature Communications **15**, 3866 (2024).

[11] I. Einav, A. Escobar, J. Baker, F. Guillard, T. Faug, Experimental confirmation of secondary flows in granular media, PREPRINT (2024). https://doi.org/10.21203/rs.3.rs-5123871/v1

[12] A. Sauret, N. Balmforth, C. Caulfield, J. McElwaine, J. Fluid Mech. **748**, 143 (2014).

[13] N. Gravish, P.B. Umbanhowar, D.I. Goldman, Phys. Rev. E **89**, 042202 (2014).

[14] E.L. Krinitzsky, Radiography in the earth sciences and soil mechanics (Springer Science & Business Media, 2012)

[15] J. Baker, F. Guillard, B. Marks, I. Einav, Nat. Commun. **9**, 5119 (2018).

[16] Smilauer et al., Yade Documentation 3rd ed. (The Yade Project, 2021), http://yade-dem.org/doc/

[17] L. Pournin, T.M. Liebling, A. Mocellin, Phys. Rev. E **65**, 011302 (2001).

[18] W.G. Hoover, C.G. Hoover, Phys. Rev. E **73**, 016702 (2006).

[19] P. Rognon, T. Miller, I. Einav, Granular Matter **17**, 177 (2015).

[20] T. Barker, D. Schaeffer, M. Shearer, J. Gray, Proc. R. Soc. A. **473**, 20160846 (2017).